PAPER

Magnetic anisotropy of 3 nm diameter Co nanowires embedded in $CeO_2/SrTiO_3(001)$: a ferromagnetic resonance study

To cite this article: P Schio *et al* 2014 *Mater. Res. Express* **1** 035015

Materials Research
Express

Magnetic anisotropy of 3 nm diameter Co nanowires embedded in $CeO_2/SrTiO_3(001)$: a ferromagnetic resonance study

P Schio[1,2,3,6], M Barturen[1,2,4,5], J Milano[1,2,4,5], F J Bonilla[1,2,4], Y Zheng[1,2,4], F Vidal[1,2,4] and A J A de Oliveira[3]

[1] Sorbonne Universités, UPMC Univ Paris 06, UMR 7588, INSP, 4 place Jussieu, F-75005, Paris, France
[2] CNRS, UMR 7588, Institut des NanoSciences de Paris, 4 place Jussieu, F-75005, Paris, France
[3] Departamento de Física, UFSCar, C P 676, 13565–905 São Carlos, São Paulo, Brazil
[4] LIFAN, Laboratoire International Franco-Argentin en Nanosciences Argentina and France
[5] CNEA-CONICET and Instituto Balseiro, UNCU CAB (R8402AGP) San Carlos de Bariloche, RN, Argentina
E-mail: pedro.schio@lnls.br and vidal@insp.jussieu.fr

Received 20 January 2014, revised 25 April 2014
Accepted for publication 25 June 2014
Published 22 July 2014

Materials Research Express **1** (2014) 035015

doi:10.1088/2053-1591/1/3/035015

Abstract

The magnetic anisotropy of 3-nm wide cobalt nanowires embedded in epitaxial $CeO_2/SrTiO_3(001)$ layers is investigated by ferromagnetic resonance measurements. The measured magnetic shape and the magnetocrystalline anisotropies confirm that the Co nanowires have their main axes perpendicular to the film surface, and they are composed of hcp Co grains with the c-axes oriented along one of the $\langle 111 \rangle$ directions of the CeO_2 matrix. The effects of such a peculiar structure on the magnetic anisotropy are addressed experimentally. The results show that the magnetic anisotropy of the wires is dominated by the magnetostatic term. The inhomogeneous structure of the wires leads to an effective magnetocrystalline anisotropy smaller than the bulk value of hcp Co.

Keywords: magnetic nanowires, ferromagnetic resonance, magnetic anisotropy

1. Introduction

Ferromagnetic nanowires (FNWs) assemblies have been studied intensively in recent years. Due to the large aspect ratio of FNWs, the magnetic anisotropy of these systems is usually dominated by shape anisotropy, leading to two stable states of the magnetization, i.e. pointing

[6] Present address: Laboratório Nacional de Luz Síncrotron, Campinas, São Paulo 13083–970, CP 6192 Brazil

up or down along the axis of the wires. This property has the potential to be applied in data storage devices with increased density [1–5]. However, other sources of magnetic anisotropy may be present, resulting in less obvious magnetic configurations, such as the so-called *snake* state observed in cobalt wires where the magnetocrystalline anisotropy competes with shape anisotropy [6–8]. Thus, a full understanding of the magnetic properties of FNWs requires determining their structure in order to unravel the different—and possibly competing—magnetic anisotropies present in the system [6, 9–13]. Also, the use of techniques sensitive to the magnetic anisotropy such as ferromagnetic resonance (FMR) is needed in order to measure the magnetic anisotropy constants of the system [14–25].

In this paper, we report on the study of the magnetic properties of cobalt nanowires embedded in CeO_2 epitaxial films grown on $SrTiO_3$(001) by pulsed laser deposition [26–28]. The nanowires are made of grains of hcp Co oriented along well-defined directions of the CeO_2 matrix and separated by fcc regions [29, 30]. This leads to a local competition of magnetostatic and magnetocrystalline anisotropies that we address here experimentally by FMR.

This paper is organized as follows. In section II we first provide some information on the growth method and on the structure of the FNWs assembly studied here. The experimental details on the ferromagnetic resonance technique are given in the same section. The FMR results and their analysis are reported in section III. Section IV is devoted to the discussion of the FMR results.

2. Experimental

2.1. Growth and structure

Cobalt containing CeO_2 epilayers were grown on $SrTiO_3$(001) substrates by pulsed laser deposition (PLD) using a KrF laser (wavelength 248 nm) operating at 2 Hz. CoO and CeO_2 targets were used. The epilayer was grown at a pressure lower than 10^{-5} mbar and 600 °C using a combinatorial procedure [31–33]: a sequence of 3 laser shots on CoO and 17 laser shots on CeO_2 was repeated until a 300 nm thickness was reached.

Using this procedure leads to the self-assembly of Co nanowires embedded in a CeO_2/$SrTiO_3$(001) epitaxial matrix, as sketched in figure 1(a). The FNWs have their axis pointing along the growth direction and the sample studied here presents a narrow distribution of diameter size centered in 3 nm. The FNW structure could be determined using high resolution transmission electron microscopy [29]: the FNWs are made of hcp Co grains with length of the order of 9 nm separated by fcc regions. The fcc regions are epitaxied in the matrix (cube-on-cube epitaxy). In the hcp grains, the *c*-axis is aligned within ±3° with one of the four ⟨111⟩ directions of the CeO_2 matrix, see figure 1(b). Considering the angle between a ⟨111⟩ and a ⟨001⟩ directions (54.7°), and the slight dispersion in *c*-axis orientation observed in the sample, the angle between the *c*-axis and the FNWs axis is 55 ± 3°.

Contrary to fcc Co, hcp Co has a strong uniaxial magneto-crystalline anisotropy, K_{1u}, directed along the *c* axis. K_{1u} has an almost constant value of 7.6×10^5 J.m^{-3} at low temperatures up to approximately 150 K [34]. It is of the same order of magnitude as the shape anisotropy, K_S, obtained when considering an infinitely long Co wire: $K_S = (\mu_0/4)M_S^2 = 6.6\times10^5$ J.m^{-3} (M_S is the saturation magnetization). As both energies fall in the same range, it is expected that they will compete within the hcp grains.

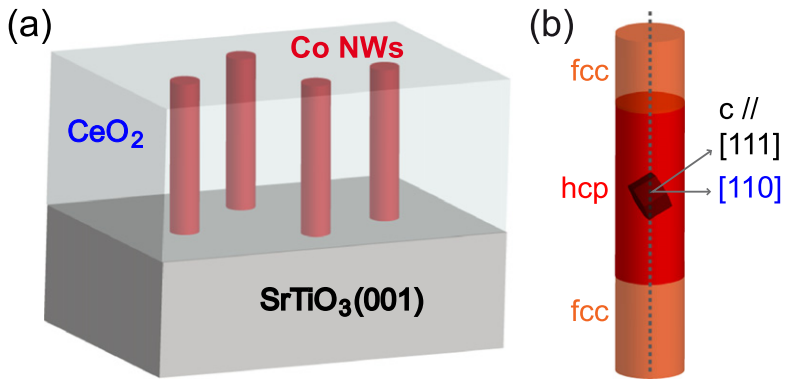

Figure 1. (a) Schematic representation of the FNWs assembly studied in this paper: the Co nanowires are embedded in an epitaxial $CeO_2/SrTiO_3(001)$ matrix with their axis pointing along [001]. (b) Schematic representation of the local, nanometer-scale, structure of the Co wires: hcp grains with c-axis oriented along one of the $\langle 111 \rangle$ directions of the matrix are separated by fcc regions.

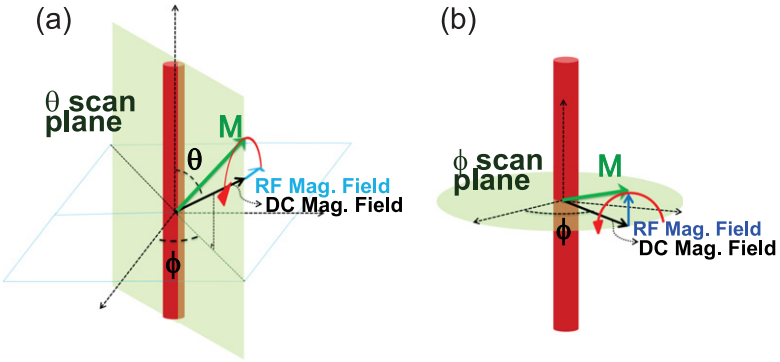

Figure 2. Schematic of FMR measurements for our samples exhibiting the two geometries of measurements: (a) θ-scan and (b) ϕ-scan. For θ-scan, it is possible to perform measurements with different ϕ angles.

2.2. FMR measurements

Ferromagnetic resonance was performed in Q-band (~34 GHz) using a Bruker ESP-300 spectrometer. The frequency was chosen to reach the resonance conditions of the Co FNWs. Considering thin film samples, there are two possible geometries to perform a magnetic resonance measurement: (*i*) the θ-scan, in which the resonance fields probed lie in a plane perpendicular to the film surface; and (*ii*) the ϕ-scan in which the sample surface plane is probed. In both geometries an angular sweep is performed in the plane probed by the measurement.

Figures 2(a) and (b) present the measurement geometries, i.e., the applied magnetic field and the plane probed in ϕ- and θ-scans for the case of nanowires lying perpendicular to the surface of thin films. The dc applied magnetic field in the FMR setup is always in the plane probed while the RF field is perpendicular to this plane. In our experiments, $\phi = 0^\circ$ and $\theta = 90^\circ$ correspond to a field applied in a direction parallel to one of the $\langle 110 \rangle$ directions of the sample.

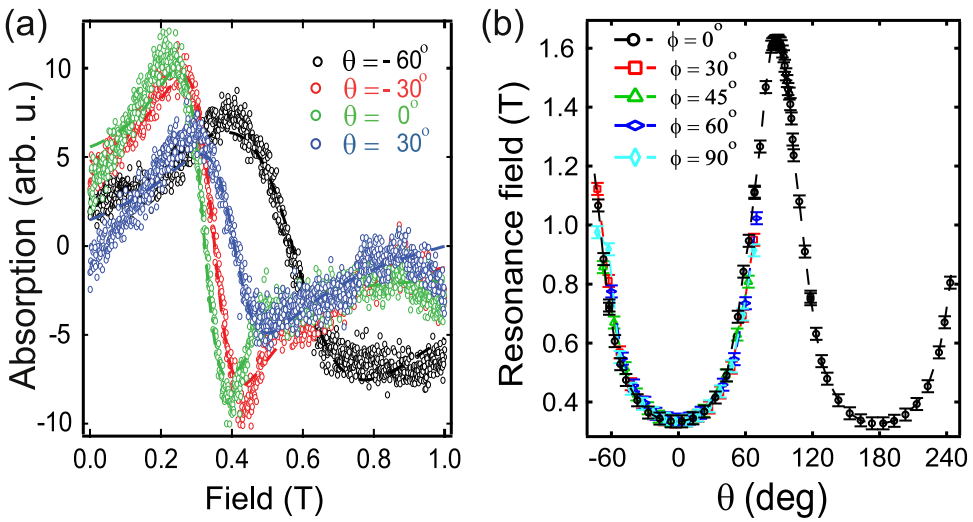

Figure 3. (a) FMR spectra of the FNWs assembly for selected values of θ, as indicated, and $\phi = 0^{\circ}$. Symbols are experimental points and dashed lines are fits considering a Lorentzian derivative. (b) Resonance field as a function of θ for distinct ϕ angles.

3. Ferromagnetic resonance study

3.1. FMR spectra

FMR spectra were recorded at room temperature in θ-scan and ϕ-scan geometries. Selected spectra obtained in θ-scan geometry at $\phi = 0^{\circ}$ are presented in figure 3(a). The variation of the resonance field with the angle of the applied magnetic field was extracted by fitting the signal considering a Lorentzian derivative function. The extracted resonance fields are presented in figure 3(b).

The large difference between the resonances for applied field perpendicular ($\theta = 0^{\circ}$) and parallel to the plane of the thin film ($\theta = 90^{\circ}$) allows us to confirm the large anisotropy in the system with an easy axis perpendicular to its surface. Such anisotropy is expected considering the high aspect ratio and orientation of the FNW [35]. In contrast, no dependence of the resonance field on the ϕ angle could be detected in this geometry, as shown in figure 3(b). The behavior observed in θ-scan geometry is the one expected when considering the high aspect ratio of the FNWs.

In order to probe if the grain structure of the wires affects the magnetic behavior, the resonances were also probed in the ϕ-scan geometry. The results obtained in this geometry are presented in figure 4. Selected spectra, recorded at different ϕ angles, are displayed in figure 4(a). These spectra have a shape approaching that of a Lorentzian derivative, but it was not possible to fit these spectra with such a function. A more careful inspection reveals that the two lobes of the curve profile are not symmetric. This asymmetry is probably due to the fact that the saturation field of the sample in this geometry and the resonance field have close values. From figure 4(c) where the in-plane hysteresis loop is displayed, we can observe that the sample magnetization is not saturated for field values at the beginning of the resonance (~1.2 T). On the other hand, for field values equal to, or larger than, the resonance field, the magnetization is at saturation. Therefore, for the first lobe of the resonance, where the sample is not saturated, a sheared behavior is observed.

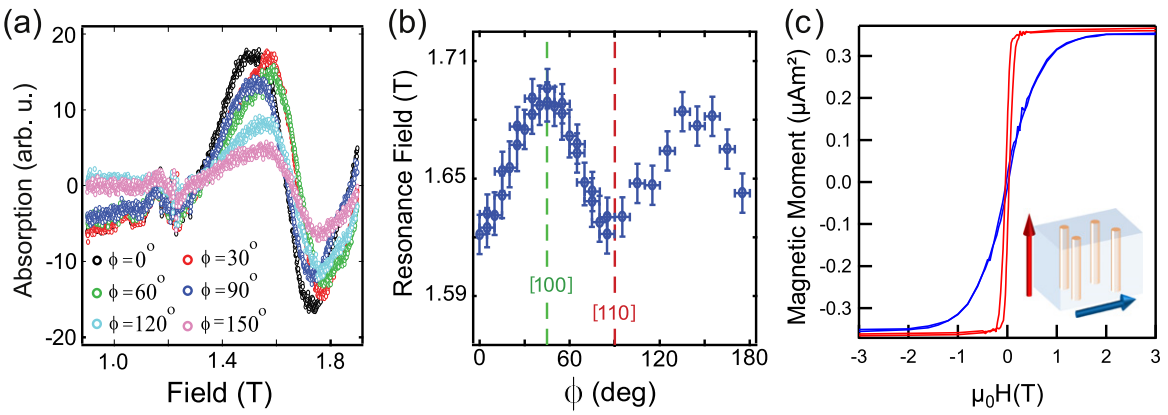

Figure 4. (a) FMR spectra in ϕ-scan geometry. (b) Variation of the resonance field with ϕ. (c) Magnetic moment versus the applied magnetic field measured at 300 K parallel and perpendicular to the film.

The resonance field variation in the plane of the thin film was determined by averaging the maximal and minimal values of the signal and is presented in figure 4(b). The observed variation indicates the presence of an additional source of anisotropy (the uniaxial anisotropy related to shape is not the only source of anisotropy). This anisotropy has a four-fold symmetry in the plane and seems to correspond to the presence of an anisotropy typically observed in cubic materials. This anisotropy can be explained based on the peculiar structural properties of the system. As described in the previous section, the cobalt in the FNWs crystallizes in the hexagonal structure with the *c*-axis pointing preferentially in a ⟨111⟩ direction of the matrix. Thus, the projection of the magnetocrystalline anisotropy in the surface of the sample produces in-plane easy directions along ⟨110⟩ and in-plane hard directions along ⟨100⟩.

3.2. FMR analysis

In order to model the resonance fields observed in the system, simulations were performed in the framework of the Smit–Beljers formalism [36, 37]. To account for the specific texture of the grains determined by HRTEM analysis, some assumptions were made. First, we considered that the magnetic units responsible for the resonance have a cylindrical shape. Given their high aspect ratio (300 nm length, 3 nm diameter), the demagnetizing factor related to the wire axis direction is set to $N_Z = 0$.

Considering that the *c*-axis of hcp Co is parallel to a ⟨111⟩ direction of the matrix, there are 4 possible directions for the orientation of the grains. The grains are formed by only one crystallographic domain with a local magnetocrystalline anisotropy equal to K_{1u}, the uniaxial anisotropy of hcp Co. We model the response of the system as the superposition of the response obtained for each orientation: instead of wires containing the 4 types of grains with K_{1u} locally, we consider 4 types of wires with a single-crystalline structure and an effective magnetocrystalline anisotropy K_{eff}^{FMR}, as illustrated in figure 5. Using this approximation, we neglect the possible effects related to exchange at the borders of the hcp grains. Such effects are incorporated into the value of K_{eff}^{FMR}, a point that will be discussed further in the next section.

The three energetic contributions for the magnetic free energy of the system are the Zeeman energy, the magnetostatic energy, and the magnetocrystalline anisotropy. Then, the

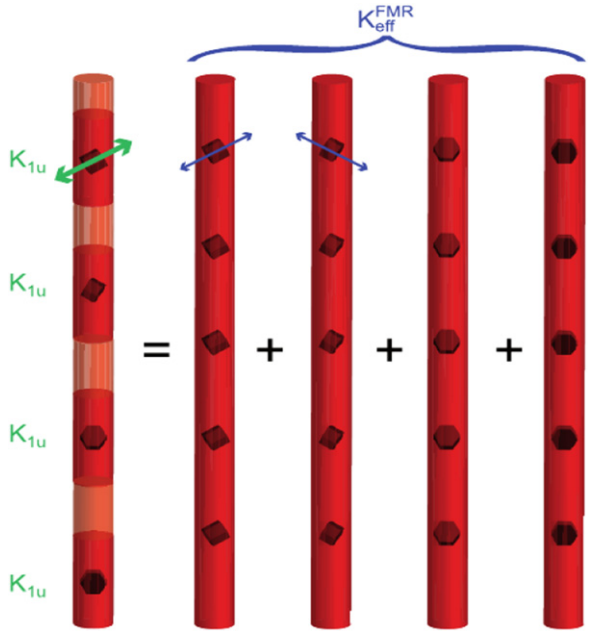

Figure 5. Schematics of the grain structure of the Co FNWs made of 4 types of hcp grains with *c*-axis parallel to the ⟨111⟩ directions of the matrix. This peculiar structure is treated in the FMR analysis as the superposition of the responses of 4 types of single crystalline wires with an effective magnetocrystalline anisotropy.

magnetic free energy used to obtain the equilibrium position of the magnetization and as an input for the resonance condition is: [14, 15]

$$F(\theta, \phi) = -\mu_0 \mathbf{M}.\mathbf{H} + \frac{\mu_0 M_S^2}{2}\left(\frac{(1-N)\sin^2\theta}{2} + N\cos^2\theta\right) - \frac{K_{eff}^{FMR}}{M_S^2}(\mathbf{G}.\mathbf{M})^2 \quad (1)$$

where $\mathbf{M} = M_S(\cos\phi\ \sin\theta, \sin\phi\ \sin\theta, \cos\theta)$ is the magnetization vector and M_S the Co bulk magnetization saturation; μ_0 is the vacuum magnetic permeability; $\mathbf{H} = H(\cos\phi_H\ \sin\theta_H, \sin\phi_H\ \sin\theta_H, \cos\theta_H)$ is the applied magnetic field with intensity H and lying in the direction described by the angles (θ_H, ϕ_H); N stands for the inter-wire magnetic coupling; [17, 38, 39] K_{eff}^{FMR} is the magnetocrystalline constant deduced from FMR modeling and $\mathbf{G}$ is a director vector of hcp *c*-axis that assumes in our case the values $\frac{1}{\sqrt{3}}(1, 1, 1)$, $\frac{1}{\sqrt{3}}(-1, 1, 1)$, $\frac{1}{\sqrt{3}}(1, -1, 1)$, $\frac{1}{\sqrt{3}}(-1, -1, 1)$ for each one of the four possible grain directions.

Using the Smit–Beljers formalism, the resonance frequency ω_R can be extracted from [36, 37]:

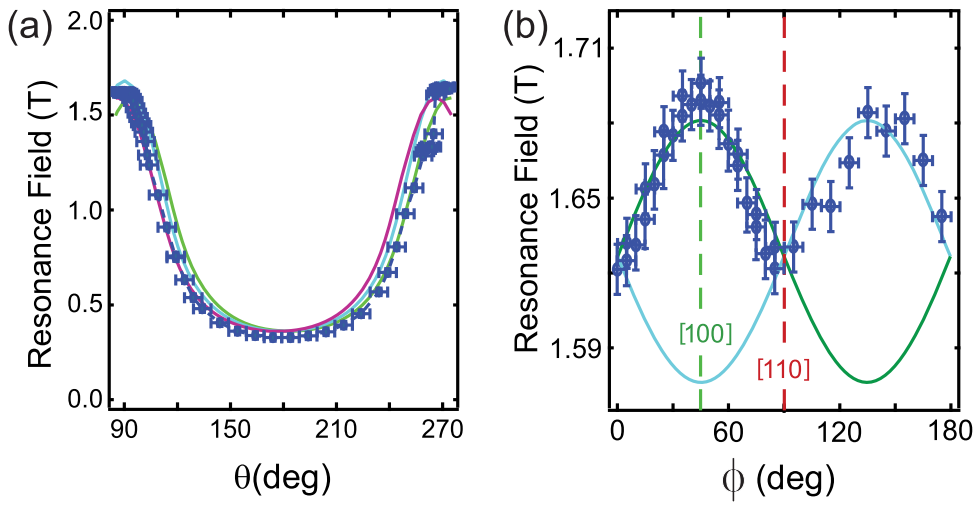

Figure 6. Comparison between the simulated results (lines) and experimental results (symbols) for $K_{1u} = 0.7 \times 10^5\,\mathrm{J/m^3}$ and $N_Z = 0.04$. For the simulated results, the different colors represent resonances of grains with different orientation.

$$\left(\frac{\omega_R}{\gamma}\right)^2 = \frac{1}{M^2 \sin^2\theta}\left(\frac{\partial^2 F(\theta,\phi)}{\partial\theta^2}\frac{\partial^2 F(\theta,\phi)}{\partial\phi^2}\right) - \frac{1}{M^2 \sin^2\theta}\left(\frac{\partial^2 F(\theta,\phi)}{\partial\theta\partial\phi}\right)^2 \tag{2}$$

where γ is a constant defined as $\gamma = \frac{g\mu_B}{\hbar}$ with g the gyromagnetic factor, μ_B the Bohr magneton and $\hbar$ the reduced Plank constant.

For θ-scan simulations, the ϕ angle was chosen in such a way that the plane probed is the plane containing a $\langle 111\rangle$ direction. The magnetization of Co derived from magnetic measurements and evaluation of the Co volume in the sample is consistent with the bulk value for hcp Co, within the error bar. The bulk value of the saturation magnetization of hcp Co ($1.424 \times 10^6\,\mathrm{A\,m^{-1}}$ at room temperature) was thus used in the simulation. It should be noted that using this value gave good agreement in previous magnetic studies [26–30]. N and K_{eff}^{FMR} are the adjustable parameters of the simulations.

The best agreement between simulation and experimental results is shown in figure 6 and was obtained for $K_{1u} = 0.7 \times 10^5\,\mathrm{J/m^3}$ and $N = 0.04$.

The simulation predicts more resonances than observed in the experiments. This is due to the fact that grains pointing in each of the four directions have different energy landscapes. Hence, the associated resonances are not necessarily equal. This is why we observe in the results of the simulations more than one resonance field for a given applied magnetic field. For example, in a plane containing $\langle 111\rangle$ and $\langle 001\rangle$ directions (θ-scan geometry) according to simulations, it would be possible to see up to three resonances at given angles and for a ϕ-scan up to two resonances would be present.

Nevertheless, the simulations performed also showed that the difference between the different resonance fields of different grains becomes negligible as the value of the magnetocrystalline constant decreases. The different resonance fields, related to grains with a

given orientation, were not experimentally observed (neither in plane nor out of plane). This issue is discussed in the next section.

Summarizing, the FMR studies of the system confirm that the magnetic behavior is dominated by shape anisotropy in the out-of-plane geometry. Moreover in the in-plane geometry the results corroborate the inner structure deduced from HRTEM analysis. In the next section we try to rationalize the value of the magnetocrystalline anisotropy contribution found by simulations.

4. Discussion

As we mentioned in subsection III.B, the dipolar coupling among wires can be considered as an effective demagnetizing field which enters the free energy expression, $F(\theta, \phi)$, by adding it to the demagnetizing energy term. In [29], we have calculated the coupling energy for a random FNWs arrangement of perfect cylindrical magnetic entities. We have found that the related anisotropy constant is 5.45×10^5 J/m^3 corresponding to $N = 0.048$. However, from the FMR best fits, we observe that the value found for N is 0.04. This fact may indicate that the dipolar coupling is slightly weaker than that obtained from the calculations. A likely reason for this behavior is that the embedded FNWs are not ideal cylinders and the terminations at the edges are not sharp enough to lead to the appearance of the magnetic charge density proposed in the model. Another reason for the dipolar coupling reduction could be the not perfectly parallel alignment of the FNWs. [27]

From the FMR analysis, we found that the magnetocrystalline anisotropy of the system is smaller than the bulk value K_{1u} if we take into account that the leading magnetocrystalline constant of hcp Co is 7.6×10^5 J/m^3 at low temperature and 4.2×10^5 J/m^3 at room temperature [34]. This may be related to the grain structure of the wires and the magnetic interplay among them, as discussed in what follows.

The effects of inhomogeneous structure and exchange coupling between the grains can be discussed considering how the spin dynamics works within the FNWs during an FMR experiment. When the resonance conditions are reached the sample is magnetically saturated. This means that the magnetic moments of different grains are parallel, there are no domain walls between grains. This fact and the existing strong coupling observed in our system lead the spins to resonance all together and, consequently, the system can be modeled like a single magnetic entity with an effective reduction of K_{1u}. We now discuss the role of exchange in a more detailed way. The exchange length, ℓ_{ex}, gives a typical value for the maximum distance between two spins that perturb each other due to exchange coupling. To understand the role of inhomogeneity and of ℓ_{ex} in the FMR response of the system, let us consider the following situation: one grain with its easy axis lying in a given direction is surrounded by other ones with their easy axis pointing in the other possible easy directions. When the spins within this grain reach the resonance condition, they start to precess. The precession will be felt by the spins belonging to the other grains (out of the resonance condition) due to the exchange coupling. The affected ones will be those that are closer than the Co exchange length, $\ell_{ex}^{Co} \sim 5$ nm [40].

The micromagnetic energy of the wires can be written as:

$$E = \int (e_{ex} + e_K + e_{MS} + e_Z) dV \tag{3}$$

where e_{ex} is the exchange energy density, e_K is the magnetocrystalline anisotropy energy density, e_{MS} is the magnetostatic energy density and e_Z is the Zeeman energy density. The effect of exchange stiffness A at the border of the grains arises because of the distinct orientation of the magnetocrystalline easy axis in neighboring grains. Labeling z the coordinate along the axis of the wire and $\mathbf{m} = \mathbf{M}/M_S$, we have $e_K = -K_{1u}(\mathbf{G}(z).\ \mathbf{m}).\ \mathbf{G}(z)$ describes the variation of the easy axis direction along the axis, i.e., the fact that it is parallel to one of the $\langle 111 \rangle$ directions of the matrix as described previously. It follows that $\mathbf{G}(z)$ exhibits abrupt variations at the border of the grains. However, as a result of the competition with exchange, $e_{ex} = A(\nabla m)^2$, the variations of $\mathbf{m}$ will be smoothed in these regions, on a length of the order of the exchange length. The resulting effective magnetocrystalline anisotropy will then be reduced compared to K_{1u}.

Taking into account this model, we propose the following expression for the energy term related to the anisotropy $K_{eff,\,ex}^{FMR}$ by averaging the grain magnetic behavior:

$$E_{K_{eff,ex}^{FMR}}(\theta,\,\phi) = -\frac{K_{gr}}{M_S^2}\sum_i w_i\,\left(\mathbf{G}_i.\ \mathbf{M}\right)^2, \tag{4}$$

where K_{gr} is the magnetic anisotropy of each grain and it is generally assumed to be equal to K_{1u}. i labels the grains with precessing spins. w_i stands for the weight of each term which is proportional to the amount of precessing spins in each grain. The weight for each grains depends on the ratio of the grain length (estimated to ~9 nm for our sample) and ℓ_{ex}^{Co} (~5 nm). For the precessing spins that belong to the grain that reaches the resonance conditions ($i = 0$) we take a value similar to the grain length. For the other grains (i = 1,2,3), the spins that also precess are those that are located at a distance shorter than ℓ_{ex}^{Co}, so we take this value to calculate the weights. Finally, by normalizing to the total length of the FNW with precessing spins we find the w_i factors (w_0 = 9/24, $w_{i=1,2,3}$ = 5/24). Then, it is possible to map to equation (4) in a single contribution of the precessing grains with an averaged anisotropy, $K_{eff,\,ex}^{FMR}$:

$$E_{K_{eff,ex}^{FMR}}(\theta,\,\phi) = C - \frac{K_{eff,\,ex}^{FMR}}{M_S^2}\left(\mathbf{G}_0.\ \mathbf{M}\right)^2, \tag{5}$$

where C is an angle-independent constant. Following this scheme the ratio of $K_{eff,\,ex}^{FMR}$ to K_{gr} is 0.16 which agrees very well with the ratio of 0.17 between K_{eff}^{FMR} (0.7×10^5 J/m^3) and K_{1u} (4.2×10^5 J/m^3) found by fitting. It is important to note that the observed reduction of magnetocrystalline anisotropy is also derived from the magnetization reversal study as shown in [29]. In this case, the role of exchange is observed through the domain wall width that drives the reduction of the Co hcp magnetocrystalline anisotropy [29]. On the other hand, in FMR experiments at saturation, domains walls are not present, however, the exchange length is present through the coupling between grains.

The effects on the effective magnetocrystalline anisotropy of exchange can also explain why some resonances are not seen in the FMR experiments. The different orientation would produce different resonance field only if the grains are considered separated. On the other hand, in the limit of strong coupling between grains only one resonance is expected as is observed in the experiments.

5. Conclusion

In summary, 3 nm wide Co nanowires were studied by FMR. The obtained results reinforce the structural and magnetic aspects already observed, such as the fact that the magnetic anisotropy is dominated by shape and the existence of four preferential directions for the grain structure.

Furthermore, FMR also puts in evidence that the coupling among FNWs is slightly reduced with respect to the calculated one for an FNWs planar array, possibly due to misalignment among wires and also to the fact that the magnetic entities are not perfect cylinders.

Finally, FMR shows that the magnetocrystalline anisotropy is reduced compared to the bulk one due to a direct exchange coupling among the grains.

Acknowledgments

This work has been supported by the Region Ile-de-France in the framework of C'Nano IdF. C'Nano IdF is the nanoscience competence center of Paris Region, supported by CNRS, CEA, MESR and Region Ile-de-France. We also acknowledge support from ANR, contract ANR-2011-BS04-007-01. P S acknowledges support from FAPESP grant 2007/08649-5 and A J A O acknowledges FAPESP grant 2012/24025-0.

References

[1] Skomski R 2003 *J. Phys.: Condens. Matter* **15** R841
[2] Fert A and Piraux L 1999 *J. Magn. Magn. Mater.* **200** 338
[3] Sellmyer D J, Zheng M and Skomski R 2001 *J. Phys.: Condens. Matter* **13** R433
[4] Paulus P M, Luis F, Kröll M, Schmid G and de Jongh L J 2001 *J. Magn. Magn. Mater.* **224** 180
[5] Sun L, Hao Y, Chien C-L and Searson P C 2005 *IBM J. Res. Dev.* **49** 79
[6] Liu Z, Chang P-C, Chang C-C, Galaktionov E, Bergmann G and Lu J G 2008 *Adv. Funct. Mater.* **18** 1573
[7] Bergmann G, Lu J G, Tao Y and Thompson R S 2008 *Phys. Rev.* B **77** 054415
[8] Erickson R P and Mills D L 2009 *Phys. Rev.* B **80** 214410
[9] Zheng M, Skomski R, Liu Y and Sellmyer D J 2000 *J. Phys.: Condens. Matter* **12** L497
[10] Zeng H, Skomski R, Menon L, Liu Y, Bandyopadhyay S and Sellmyer D J 2002 *Phys. Rev.* B **65** 134426
[11] Darques M, Piraux L, Encinas A, Bayle-Guillemaud P, Popa A and Ebels U 2005 *Appl. Phys. Lett.* **86** 072508
[12] Soulantica K, Wetz F, Maynadié J, Falqui A, Tan R P, Blon T, Chaudret B and Respaud M 2009 *Appl. Phys. Lett.* **95** 152504
[13] Pirota K R, Béron F, Zanchet D, Rocha T C R, Navas D, Torrejón J, Vazquez M and Knobel M 2011 *J. Appl. Phys.* **109** 083919
[14] Lederman D, Dutta P, Seehra M S and Shi H 2012 *J. Phys.: Condens. Matter* **24** 186001
[15] Varalda J *et al* 2006 *J. Phys.: Condens. Matter* **18** 9105
[16] Ebels U, Duvail J L, Wigen E, Piraux L, Buda L D and Ounadjela K 2001 *Phys. Rev.* B **64** 144421
[17] Encinas-Oropesa A, Demand M, Piraux L, Huynen I and Ebels U 2001 *Phys. Rev.* B **63** 104415
[18] Ramos C A, Brigneti E V and Vazquez M 2004 *Physica B: Condens. Matter* **354** 195
[19] Vazquez M, Hernandez-Velez M, Pirota K, Asenjo A, Navas D, Velazquez J, Vargas P and Ramos C 2004 *Eur. Phys. J.* B **40** 489
[20] Yalcin O, Yildiz F, Ozdemir M, Aktas B, Koseoglu Y, Bal M and Tuominen M T 2004 *J. Magn. Magn. Mat.* **272** 1684
[21] Dumitru I, Li F, Wiley J B, Cimpoesu D, Stancu A and Spinu L 2004 *IEEE Trans. Magn.* **41** 3361

[22] Carignan L-P, Lacroix C, Ouimet A, Ciureanu M, Yelon A and Menard D 2007 *J. Appl. Phys.* **102** 023905
[23] Pardavi-Horvath M, Si P E, Vazquez M, Rosa W O and Badini G 2008 *J. Appl. Phys.* **103** 07D517
[24] Kartopu G, Yalcin O, Kazan S and Aktas B 2009 *J. Magn. Magn. Mat.* **321** 1142
[25] Kartopu G, Yalcin O, Choy K L, Topkaya R, Kazan S and Aktas B 2011 *J. Appl. Phys.* **109** 033909
[26] Vidal F, Zheng Y, Milano J, Demaille D, Schio P, Fonda E and Vodungbo B 2009 *Appl. Phys. Lett.* **95** 152510
[27] Schio P, Vidal F, Zheng Y, Milano J, Fonda E, Demaille D, Vodungbo B, Varalda J, de Oliveira A J A and Etgens V H 2010 *Phys. Rev.* B **82** 094436
[28] Vidal F, Schio P, Keller N, Zheng Y, Demaille D, Bonilla F J, Milano J and de Oliveira A J A 2012 *Physica B: Condensed Matter* **407** 3070
[29] Vidal F, Zheng Y, Schio P, Bonilla F J, Barturen M, Milano J, Demaille D, Fonda E, de Oliveira A J A and Etgens V H 2012 *Phys. Rev. Lett.* **109** 117205
[30] Schio P, Bonilla F J, Zheng Y, Demaille D, Milano J, de Oliveira A J A and Vidal F 2013 *J. Phys.: Condens. Matter* **25** 056002
[31] Aimon N M, Kim D H, Choi H K and Ross C A 2012 *Appl. Phys. Lett.* **100** 092901
[32] Liu H-J *et al* 2012 *ACS Nano* **6** 6952
[33] Bonilla F J *et al* 2013 *ACS Nano* **7** 4022
[34] Ono F and Maeta H 1989 *Physica* B **161** 134
[35] Chipara M, Skomski R, Kirby R and Sellmyer D J 2011 *J. Mater. Res.* **26** 2169
[36] Smit J and Beljers H-G 1955 *Philips Res. Rep.* **10** 113
[37] Lindner J and Farle M 2003 (*Magnetic Anisotropy of Heterostructures In Magnetic Heterostructures Springer Tracts in Modern Physics* vol 227) ed H Zabel and S D Bader (Berlin: Springer) p 57, chapter 2
[38] Zighem F, Maurer T, Ott F and Chaboussant G 2011 *J. Appl. Phys.* **109** 013910
[39] Vega V, Böhnert T, Martens S, Waleczek M, Montero-Moreno J M, Görlitz D, Prida V M and Nielsch K 2012 *Nanotechnology* **23** 465709
[40] Kronmüller H and Fähnle M 2003 *Micromagnetism and the Microstructure of Ferromagnetic Solids* (Cambridge: Cambridge University Press) p 48, chapter 3